PERGAMON

Engineering Fracture Mechanics 69 (2002) 95–112

Engineering Fracture Mechanics

www.elsevier.com/locate/engfracmech

Fracture in quasi-brittle materials: a review of continuum damage-based approaches

René de Borst *

Faculty of Aerospace Engineering/Koiter Institute Delft, Delft University of Technology, P.O. Box 5058, NL-2600 GB Delft, Netherlands

Abstract

Starting from the early ideas on smeared-crack modelling of quasi-brittle materials (concrete, rock) as pioneered in the late 1960s various refinements are discussed such as the shear retention factor, the tension-stiffening concept and the tension-softening concept. Next, smeared-crack models are put in the unified context of damage mechanics together with the multiple-smeared crack approach and the (closely) related microplane damage models. The concept of fracture energy is introduced for tensile and compressive loadings and is also elaborated for reinforced concrete. A concise summary is given of recent finite element concepts for cohesive-zone models (fracture energy models). © 2001 Elsevier Science Ltd. All rights reserved.

Keywords: Concrete fracture; Damage; Smeared cracking; Localisation; Cohesive-zone models; Fracture energy; Tension-softening; Tension-stiffening; Reinforcement

1. Introduction

Numerical modelling of plain and reinforced concrete started in the late 1960s with the landmark papers of Rashid [1] and of Ngo and Scordelis [2] in which the smeared and discrete crack models were introduced. Especially the first approach has gained much popularity, and in the 1970s comprehensive efforts were invested in developing smeared-crack models which could reproduce the experimentally observed stress–strain characteristics of concrete. Two major modifications were introduced, namely the so-called shear retention factor [3], and the replacement of the sudden stress drop upon crack initiation by a descending branch in the tensile stress–strain relation to represent the contribution of the stiffness of the concrete between the cracks in reinforced applications (*tension-stiffening*).

In the early 1980s we have witnessed a number of important further developments. Firstly, there has been the recognition, originally by Cope et al. [4], that the introduction of a shear retention factor causes the principal stresses in a cracked integration point to rotate upon further loading. Moreover, in combination with a descending branch in the tensile stress–strain diagram, the major tensile stress may (easily) exceed the tensile strength in another direction than the one normal to the crack if the crack is fixed in a

* Tel.: +31-15-278-5464.
E-mail address: r.deborst@lr.tudelft.nl (R. de Borst).

0013-7944/02/$ - see front matter
PII: S0013-7944(01)00082-0

certain direction. Without the use of a shear retention factor this cannot happen, and the importance of this phenomenon has initially been overlooked when the shear retention factor was introduced.

Another most important issue was the recognition that plain concrete is not a perfectly brittle material in the Griffith sense, but that it has some residual load-carrying capacity after reaching the tensile strength. This experimental observation has led to the replacement of purely brittle crack models by *tension-softening* models, in which a descending branch was introduced to model the gradually diminishing tensile strength of concrete upon further crack opening. Such a descending branch also emerges in most tension-stiffening models and much confusion has existed ever since about how to model tension-softening and tension-stiffening in reinforced concrete in a rational manner.

The introduction of tension softening in crack models was also motivated on theoretical grounds. It was observed that the use of strength models [5] or the straightforward use of strain-softening models led to an unacceptable and unphysical mesh sensitivity [6,7]. A similar observation had been made for discrete crack models, and probably motivated by the Dugdale–Barenblatt cohesive crack models [8,9], Hillerborg proposed as early as in 1976 his landmark paper in which he introduced the Fictitious Crack Model [10], which ensured a mesh-independent energy release upon crack propagation. Adapting this concept to smeared formulations, Bažant and Oh [11] introduced the crack band model, in which the fracture energy introduced by Hillerborg was smeared out over the width of the area in which the crack *localises*, for lower-order elements typically equal to the width of one element.

During the 1980s some alternative approaches were also pioneered. Primarily driven by the French school, damage mechanics concepts were used for modelling cracking in reinforced concrete [12,13], while Bažant and co-workers adapted the early ideas of Batdorf and Budiansky [14] on metal plasticity to fracture in concrete and rock and developed a class of microplane models [15,16]. Finally, Feenstra and de Borst [17–19] formulated a class of plasticity theories geared towards describing cracking in concrete and rock, with the principal aim to avoid the dual approach that in tension smeared-crack models were used, while in compression plasticity theories were employed to describe crushing.

In this contribution, we shall first follow the historical developments of the smeared-crack models, noting the merits and disadvantages of the various ideas and the propositions to remedy certain deficiencies. Then, we will rigorously cast the smeared-crack models into a damage format and show that they can be conceived as a special case of anisotropic damage models. Also, the relation with the microplane models with a damage type stress–strain relation on a microplane will be elucidated. A consistent tangential stiffness matrix is derived for use within Newton–Raphson algorithms in a finite element context.

In the second part of the paper, the issue of convergence of numerical computations towards a physically realistic solution will be discussed. The concept of cohesive zones (fracture energy models), which has been discussed briefly in the first part, is taken up and elaborated, also for compressive failure and for reinforced concrete. The treatment includes a concise discussion of contemporary finite element concepts to embed cohesive-zone models in smeared formulations.

2. Elementary smeared-crack concepts

Prior to cracking, quasi-brittle materials like concrete and rock can, for many purposes, be modelled sufficiently accurately as isotropic, linear-elastic. For instance, in a two-dimensional state of stress we have

$$\begin{bmatrix} \sigma_{xx} \\ \sigma_{yy} \\ \sigma_{xy} \end{bmatrix} = \frac{E}{1-\nu^2} \begin{bmatrix} 1 & \nu & 0 \\ \nu & 1 & 0 \\ 0 & 0 & 1/2(1-\nu) \end{bmatrix} \begin{bmatrix} \varepsilon_{xx} \\ \varepsilon_{yy} \\ \gamma_{xy} \end{bmatrix} \tag{1}$$

When the major principal tensile stress exceeds the tensile strength or, in more generally, when the combination of principal stresses violates a tension cut-off criterion, a crack is initiated perpendicular to the

direction of the principal stress. This embodies that in a sampling point, where the stress, strain and history variables are monitored, the isotropic stress–strain relation is replaced by an orthotropic law with the n, s-axes the axes of orthotropy, where n is the direction normal to the crack (mode-I) and s refers to the direction tangential to the crack (mode-II). In a first attempt the orthotropic relation can be defined as [1]:

$$\begin{bmatrix} \sigma_{nn} \\ \sigma_{ss} \\ \sigma_{ns} \end{bmatrix} = \begin{bmatrix} 0 & 0 & 0 \\ 0 & E & 0 \\ 0 & 0 & 0 \end{bmatrix} \begin{bmatrix} \varepsilon_{nn} \\ \varepsilon_{ss} \\ \gamma_{ns} \end{bmatrix} \tag{2}$$

where the orthotropic stress–strain relation has been set up in the coordinate system that aligns with the axes of orthotropy. Eq. (2) shows that both the normal stiffness and the shear stiffness across the crack are set equal to zero upon cracking. As a consequence all effects of lateral contraction/expansion also disappear.

If, for a plane-stress situation, $\boldsymbol{\sigma}_{ns} = [\sigma_{nn}, \sigma_{ss}, \sigma_{ns}]^{\mathrm{T}}$ and $\boldsymbol{\varepsilon}_{ns} = [\varepsilon_{nn}, \varepsilon_{ss}, \gamma_{ns}]^{\mathrm{T}}$, and the secant stiffness matrix $\mathbf{D}^{\mathrm{s}}_{ns}$ is defined as

$$\mathbf{D}^{\mathrm{s}}_{ns} = \begin{bmatrix} 0 & 0 & 0 \\ 0 & E & 0 \\ 0 & 0 & 0 \end{bmatrix} \tag{3}$$

we can write the orthotropic elastic stiffness relation in the n, s-coordinate system as

$$\boldsymbol{\sigma}_{ns} = \mathbf{D}^{\mathrm{s}}_{ns}\boldsymbol{\varepsilon}_{ns} \tag{4}$$

If we introduce ϕ as the angle from the x-axis to the n-axis, we can relate the components of $\boldsymbol{\varepsilon}_{ns}$ and $\boldsymbol{\sigma}_{ns}$ to those in the global x, y-coordinate via the standard transformation matrices $\mathbf{T}_{\varepsilon}$ and $\mathbf{T}_{\sigma}$:

$$\boldsymbol{\varepsilon}_{ns} = \mathbf{T}_{\varepsilon}(\phi)\boldsymbol{\varepsilon}_{xy} \tag{5}$$

and

$$\boldsymbol{\sigma}_{ns} = \mathbf{T}_{\sigma}(\phi)\boldsymbol{\sigma}_{xy} \tag{6}$$

The local secant stiffness relation (4) then transforms into a secant stiffness relation in the global x, y-coordinate system:

$$\boldsymbol{\sigma}_{xy} = \mathbf{T}^{-1}_{\sigma}(\phi)\mathbf{D}^{\mathrm{s}}_{ns}\mathbf{T}_{\varepsilon}(\phi)\boldsymbol{\varepsilon}_{xy} \tag{7}$$

The special case that ϕ is fixed upon crack initiation, i.e. when the tension cut-off criterion is first reached, is known as the *fixed smeared-crack model*. When we refer to this angle as ϕ_0, we have instead of Eq. (7),

$$\boldsymbol{\sigma}_{xy} = \mathbf{T}^{-1}_{\sigma}(\phi_0)\mathbf{D}^{\mathrm{s}}_{ns}\mathbf{T}_{\varepsilon}(\phi_0)\boldsymbol{\varepsilon}_{xy} \tag{8}$$

Because of ill-conditioning, use of Eq. (2) may result in premature convergence difficulties. Also, physically unrealistic and distorted crack patterns can be obtained, e.g. Ref. [3]. For this reason a reduced shear modulus βG $(0 \leqslant \beta \leqslant 1)$ was reinserted in the model:

$$\mathbf{D}^{\mathrm{s}}_{ns} = \begin{bmatrix} 0 & 0 & 0 \\ 0 & E & 0 \\ 0 & 0 & \beta G \end{bmatrix} \tag{9}$$

The use of the so-called *shear retention factor* β not only reduces the numerical difficulties, but it also improves the physical reality of fixed crack models, because it can be thought of as a model representation of aggregate interlock. Most researchers simply adopt a constant shear retention factor ($\beta = 0.2$ is a commonly adopted value) but sometimes a crack-strain dependent factor is employed [20]. The latter

option is more realistic since the capability of a crack to transfer shear stresses in mode-II decreases with increasing crack strain.

The fact that the stiffness normal to the crack in Eq. (9) is set equal to zero involves a sudden drop of the tensile stress from the initial tensile strength f_t to zero upon crack initiation. Similar to the use of a zero shear retention factor, this may cause numerical problems. Moreover, careful servo-controlled experiments on plain concrete have shown that concrete is not a perfectly brittle material in the Griffith sense, but that it has some residual load-carrying capacity after reaching the tensile strength. This experimental observation has led to the replacement of purely brittle crack models by *tension-softening* models, in which a descending branch was introduced to model the gradually diminishing tensile strength of concrete upon further crack opening. In a smeared context, one can model this by inserting a normal reduction factor μ in the secant stiffness matrix:

$$\mathbf{D}_{ns}^{s} = \begin{bmatrix} \mu E & 0 & 0 \\ 0 & E & 0 \\ 0 & 0 & \beta G \end{bmatrix} \tag{10}$$

where, similar to the shear reduction factor β, the normal reduction factor μ can be a function of the strain normal to the crack: $\mu = \mu(\varepsilon_{nn})$. A final refinement is given by the addition of Poisson coupling after crack formation. Then, we arrive at the mode-I crack band formulation of Bažant and Oh [11] extended with mode-II shear retention:

$$\mathbf{D}_{ns}^{s} = \begin{bmatrix} \frac{\mu E}{1-\nu^2\mu} & \frac{\nu\mu E}{1-\nu^2\mu} & 0 \\ \frac{\nu\mu E}{1-\nu^2\mu} & \frac{E}{1-\nu^2\mu} & 0 \\ 0 & 0 & \beta G \end{bmatrix} \tag{11}$$

Crack models as discussed in the preceding are based on total strain concepts. An injective relation is assumed between the stress $\boldsymbol{\sigma}$ and the total strain $\boldsymbol{\varepsilon}$. This approach works well in many applications, but it has some drawbacks. Firstly, it is impossible to properly combine cracking and other non-linear phenomena (e.g., creep, shrinkage, thermal effects) when a total relation is adopted between stress and strain. To overcome this difficulty de Borst and co-workers [21–23] have proposed a model in which the total strain is additively decomposed into a concrete part $\boldsymbol{\varepsilon}^{co}$ and a crack part $\boldsymbol{\varepsilon}^{cr}$:

$$\boldsymbol{\varepsilon} = \boldsymbol{\varepsilon}^{co} + \boldsymbol{\varepsilon}^{cr} \tag{12}$$

The concrete strain can then be composed of an elastic contribution, a shrinkage contribution, a creep contribution and so on. Similarly, the crack strain can be decomposed further, so that:

$$\boldsymbol{\varepsilon}^{cr} = \boldsymbol{\varepsilon}_1^{cr} + \boldsymbol{\varepsilon}_2^{cr} + \cdots \tag{13}$$

where $\boldsymbol{\varepsilon}_1^{cr}$ is the strain owing to a primary crack, $\boldsymbol{\varepsilon}_2^{cr}$ is the strain owing to a secondary crack and so on.

In this fashion also another deficiency can be remedied of the smeared-crack model with a single crack. In the elaboration of this model it has been assumed that upon violation of the tension cut-off the direction of the crack plane is fixed. During subsequent loading shear strains may then arise along the crack plane, which, in turn, will lead to a build-up of shear stresses over the crack plane. When a softening model is used the residual normal stress that acts over a crack and the shear stress over that crack can cause the principal stresses to exceed the tensile strength in the new principal direction, which is different from the direction normal to the existing crack plane. Eq. (13) allows the initiation of a secondary crack, which thus remedies the above anomaly.

Another way to achieve this goal is to depart from the concept that the crack direction is fixed upon initiation. In this so-called *rotating crack model*, originally proposed by Cope et al. [4], the major principal stress direction and the normal to the crack are aligned during the entire cracking process. The local n, s-coordinate system is now the same coordinate system as that of the principal values of the stress tensor.

Consequently, the shear stress σ_{nt} is always zero. Thus, an explicit shear stiffness term as in the fixed crack model is not possible in the rotating crack concept as a tangential shear stiffness term implicitly evolves from the rotation of the principal stress axes.

In principle, the normal reduction factor μ can be determined from a simple tensile test. However, a straightforward translation from experimental data in an expression for μ leads to results that are not objective with regard to mesh refinement [6,7]. To overcome this problem, it has been proposed to consider the fracture energy G_f as a basic material parameter. The fracture energy is defined as the amount of energy needed to create one unit of area of a continuous crack and is the fundamental quantity that governs crack propagation. This so-called 'tension-softening' model should not be confused with the 'tension-stiffening' model. Both models lead to 'softening', in the sense that they introduce a gradual decrease of the load-carrying capacity, i.e. the tensile strength f_t. However, the softening nature of the tension-softening model originates from the gradual loss of integrity of concrete or rock in tension, whereas the tension-stiffening model represents the stiffness contribution of concrete between the cracks to the composite material 'reinforced concrete'.

3. A damage mechanics framework

So far, the treatment of smeared-crack models has been rather elementary. We will now present a more formal treatment, which shows that the fixed and rotating smeared-crack models, but also microplane models, can be conceived as a special case of (anisotropic) damage models.

The basic structure of constitutive models that are set up in the spirit of damage mechanics is simple. We have a total stress–strain relation,

$$\sigma_{ij} = D^{s}_{ijkl}(q_m, \omega_{mn}, \Omega_{mnop}, \ldots)\varepsilon_{kl} \tag{14}$$

where σ_{ij} is the stress tensor, ε_{kl} is the strain tensor and D^{s}_{ijkl} is a secant stiffness tensor, which can depend on a number of internal variables, like scalar-valued internal variables q_m, and tensor-valued internal variables like ω_{mn}, Ω_{mnop} and so on. Relation (14) distinguishes itself from classical nonlinear elasticity by a history dependence, which is incorporated via a loading–unloading function, f, which vanishes upon loading, and is negative otherwise. For damage growth, f must remain zero for an infinitesimal period, so that we have the additional requirement that $\dot{f} = 0$. The theory is completed by specifying the appropriate (material-dependent) evolution equations for the internal variables.

3.1. Isotropic damage models

For the case of isotropic damage evolution, the total stress–strain relation (14) specialises as

$$\sigma_{ij} = [(1-\omega_1)G(\delta_{ik}\delta_{jl} + \delta_{il}\delta_{jk} - (2/3)\delta_{ij}\delta_{kl}) + (1-\omega_2)K\delta_{ij}\delta_{kl}]\varepsilon_{kl} \tag{15}$$

with G the virgin shear modulus and K the virgin bulk modulus, which are degraded by the scalar damage variables ω_1 and ω_2, respectively. A further simplification can be achieved if it is assumed that the secant shear stiffness and bulk moduli, $(1-\omega_1)G$ and $(1-\omega_2)K$, degrade in the same manner during damage growth. Essentially, this means that Poisson's ratio ν remains constant throughout the damage process and we have

$$\sigma_{ij} = (1-\omega)D^{e}_{ijkl}\varepsilon_{kl} \tag{16}$$

with ω the damage variable which grows from zero to one (at complete loss of integrity) and D^{e}_{ijkl} the fourth-order elastic stiffness tensor. The total stress–strain relation (16) is again complemented by a damage loading function f, which now reads: $f = f(\tilde{\varepsilon}, \tilde{\sigma}, \kappa)$, with $\tilde{\varepsilon}$ and $\tilde{\sigma}$ scalar-valued functions of the strain and

stress tensors, respectively, and κ the only remaining scalar history variable. The damage loading function f and the rate of the history variable, $\dot{\kappa}$, have to satisfy the discrete Kuhn–Tucker loading–unloading conditions

$$f \leqslant 0, \quad \dot{\kappa} \geqslant 0, \quad f\dot{\kappa} = 0 \tag{17}$$

In this contribution we consider the case that the damage loading function does not depend on $\tilde{\sigma}$. Then,

$$f(\tilde{\varepsilon}, \kappa) = \tilde{\varepsilon} - \kappa \tag{18}$$

For metals a commonly accepted choice for $\tilde{\varepsilon}$ is [24]:

$$\tilde{\varepsilon} = (1/2)\varepsilon_{ij} D^{\mathrm{e}}_{ijkl} \varepsilon_{kl} \tag{19}$$

Eq. (19) is less convenient from the point of view that it does not reduce to the uniaxial strain for uniaxial stressing. For this reason it is sometimes replaced by the modified expression

$$\tilde{\varepsilon} = \sqrt{\frac{1}{E}\varepsilon_{ij} D^{\mathrm{e}}_{ijkl} \varepsilon_{kl}} \tag{20}$$

with E the virgin Young's modulus. Expression (20) is represented graphically in the principal strain space for plane-stress conditions in Fig. 1(a). In this figure, a scaling has been applied such that $\tilde{\varepsilon} = 1$, while $\nu = 0.2$. The dashed lines are uniaxial stress paths. The above energy release rate definition for $\tilde{\varepsilon}$ gives equal weights to tensile and compressive strain components, which makes it unsuitable to describe the mechanical behaviour of quasi-brittle materials like concrete and rock. To remedy this deficiency, Mazars and Pijaudier-Cabot [12,13] have suggested the definition

$$\tilde{\varepsilon} = \sqrt{\sum_{i=1}^{3} \left(\langle \varepsilon_i \rangle\right)^2} \tag{21}$$

with ε_i the principal strains, and $\langle \varepsilon_i \rangle = \varepsilon_i$ if $\varepsilon_i > 0$ and $\langle \varepsilon_i \rangle = 0$ otherwise. A contour plot for $\tilde{\varepsilon} = 1$ is given in Fig. 1(b). A third definition for the equivalent strain has been proposed by de Vree et al. [25]. This proposition, which can be named a modified von Mises definition, is given by

$$\tilde{\varepsilon} = \frac{k-1}{2k(1-\nu)} I_1 + \frac{1}{2k}\sqrt{\frac{(k-1)^2}{(1-2\nu)^2} I_1^2 + \frac{6k}{(1+\nu)^2} J_2} \tag{22}$$

with $I_1 = \varepsilon_{kk}$ the first invariant of the strain tensor and $J_2 = e_{ij}e_{ij}$ the second invariant of the deviatoric strain tensor $e_{ij} = \varepsilon_{ij} - (1/3)\varepsilon_{kk}$. The parameter k governs the sensitivity of the compressive strain components relative to the tensile strain components. The definition of $\tilde{\varepsilon}$ is such that a compressive uniaxial stress $k\sigma$ has the same effect as a uniaxial tensile stress σ. The parameter k is therefore typically set equal to the ratio of the compressive uniaxial strength and the tensile uniaxial strength: $k = f_{\mathrm{c}}/f_{\mathrm{t}}$. A graphical representation of the modified von Mises definition is given in Fig. 1(c) for $k = 10$.

The history parameter κ starts at a damage threshold level κ_0 and is updated by the requirement that during damage growth $f = 0$. Damage growth occurs according to an evolution law such that $\omega = \omega(\kappa)$, which can be determined from a uniaxial test. For instance, for a linear elastic behaviour up to a peak tensile strength $f_{\mathrm{t}} = E\kappa_0$, followed by a linear descending branch up to a strain κ_{u} at which the load-carrying capacity is exhausted (and thus $\omega = 1$), the evolution law reads:

$$\omega(\kappa) = \frac{\kappa_{\mathrm{u}}(\kappa - \kappa_0)}{\kappa(\kappa_{\mathrm{u}} - \kappa_0)} \tag{23}$$

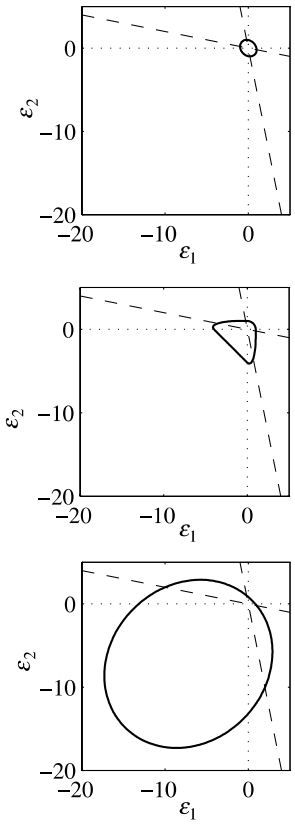

Fig. 1. Contour plots for $\tilde{\varepsilon}$ for (a) the local energy release concept, (b) the Mazars definition, and (c) the modified von Mises definition (after Ref. [45]).

3.2. Anisotropic damage models

While isotropic damage models have been used successfully for describing progressive crack propagation, their disadvantage is that possible compressive strut action is eliminated. This is a drawback especially for the analysis of reinforced concrete members. Directional dependence of damage evolution can be incorporated by degrading the Young's modulus E in a preferential direction. When, for plane-stress conditions, distinction is made between the global x, y-coordinate system and a local n, s-coordinate system a simple loading function in the local coordinate system would be

$$f(\varepsilon_{nn}, \kappa) = \varepsilon_{nn} - \kappa \tag{24}$$

with ε_{nn} the normal strain in the local n, s-coordinate system, subject to the standard Kuhn–Tucker loading–unloading conditions. The secant stiffness relation now reads

$$\boldsymbol{\sigma}_{ns} = \mathbf{D}^{\mathrm{s}}_{ns}\boldsymbol{\varepsilon}_{ns} \tag{25}$$

cf. Eq. (4), and $\mathbf{D}^{\mathrm{s}}_{ns}$ defined as

$$\mathbf{D}^{\mathrm{s}}_{ns} = \begin{bmatrix} \frac{(1-\omega_1)E}{1-(1-\omega_1)\nu^2} & \frac{(1-\omega_1)\nu E}{1-(1-\omega_1)\nu^2} & 0 \\ \frac{(1-\omega_1)\nu E}{1-(1-\omega_1)\nu^2} & \frac{E}{1-(1-\omega_1)\nu^2} & 0 \\ 0 & 0 & (1-\omega_2)G \end{bmatrix} \tag{26}$$

with $\omega_1 = \omega_1(\kappa)$ and $\omega_2 = \omega_2(\kappa)$. The factor $1-\omega_1$ represents the degradation of the normal stiffness and can be identified with the normal reduction factor μ, while the factor $1-\omega_2$ represents the degradation of the shear stiffness and can be identified with the shear retention factor β [3]. It is emphasised that because of the choice of a preferential direction in which damage takes place, the damage variables ω_1 and ω_2 have an entirely different meaning than those that were introduced in the basic isotropic formulation of Eq. (15).

With aid of the standard transformation matrices $\mathbf{T}_\varepsilon$ and $\mathbf{T}_\sigma$, cf. Eqs. (5) and (6) the damage loading function (24) can be written in terms of the strain components ε_{xx}, ε_{yy} and γ_{xy} of the global x, y-coordinate system:

$$f = \varepsilon_{xx}\cos^2\phi + \varepsilon_{yy}\sin^2\phi + \gamma_{xy}\sin\phi\cos\phi - \kappa \tag{27}$$

Similarly, we obtain for the secant stress–strain relation instead of Eq. (25):

$$\boldsymbol{\sigma}_{xy} = \mathbf{T}^{-1}_{\sigma}(\phi)\mathbf{D}^{\mathrm{s}}_{ns}\mathbf{T}_{\varepsilon}(\phi)\boldsymbol{\varepsilon}_{xy} \tag{28}$$

Eqs. (27) and (28) incorporate the traditional fixed crack model and the rotating crack model. The only difference is that in the fixed crack model the inclination angle ϕ is fixed when the major principal stress first reaches the tensile strength ($\phi = \phi_0$), while in the rotating crack concept ϕ changes such that the n-axis continues to coincide with the major principal stress direction. This difference has profound consequences when deriving the tangential stiffness, especially with regard to the shear term.

The above framework also allows for incorporation of constitutive models that are based on the microplane concept. As an example we shall consider a microplane model based on the so-called kinematic constraint, which implies that the normal and tangential strains on a microplane that is labelled α, can be derived by a simple projection of the global strains $\boldsymbol{\varepsilon}_{xy}$ similar to Eq. (5):

$$\boldsymbol{\varepsilon}^{\alpha}_{ns} = \mathbf{T}_{\varepsilon}(\phi^{\alpha})\boldsymbol{\varepsilon}_{xy} \tag{29}$$

The stresses on this microplane can be derived in a fashion similar to Eq. (25):

$$\boldsymbol{\sigma}^{\alpha}_{ns} = \mathbf{D}^{\alpha}_{ns}\boldsymbol{\varepsilon}^{\alpha}_{ns} \tag{30}$$

with $\mathbf{D}^{\alpha}_{ns}$ given by

$$\mathbf{D}^{\alpha}_{ns} = \begin{bmatrix} (1-\omega^{\alpha}_{\mathrm{N}})E_{\mathrm{N}} & 0 & 0 \\ 0 & 0 & 0 \\ 0 & 0 & (1-\omega^{\alpha}_{\mathrm{T}})E_{\mathrm{T}} \end{bmatrix} \tag{31}$$

where the initial stiffness moduli E_{N} and E_{T} are functions of the Young's modulus, the Poisson's ratio and a weight parameter, e.g. Ref. [16]. The damage parameters $\omega^{\alpha}_{\mathrm{N}}$ and $\omega^{\alpha}_{\mathrm{T}}$ for the normal stiffness and the shear stiffness are functions of the history parameters $\kappa^{\alpha}_{\mathrm{N}}$ and $\kappa^{\alpha}_{\mathrm{T}}$ in a standard fashion: $\omega^{\alpha}_{\mathrm{N}} = \omega^{\alpha}_{\mathrm{N}}(\kappa^{\alpha}_{\mathrm{N}})$ and $\omega^{\alpha}_{\mathrm{T}} = \omega^{\alpha}_{\mathrm{T}}(\kappa^{\alpha}_{\mathrm{T}})$. The main departure from the fixed crack model as outlined above is the fact that we need two damage loading functions on microplane α

$$f^{\alpha}_{\mathrm{N}} = \varepsilon^{\alpha}_{nn} - \kappa^{\alpha}_{\mathrm{N}} \tag{32}$$

and

$$f^{\alpha}_{\mathrm{T}} = \gamma^{\alpha}_{ns} - \kappa^{\alpha}_{\mathrm{T}} \tag{33}$$

each subject to the standard Kuhn–Tucker loading–unloading conditions. Finally, the stresses in the global x, y coordinate system are recovered by summing over all the microplanes and by transforming them in a standard fashion according to Eq. (6). With Eqs. (29) and (30) we finally arrive at

$$\boldsymbol{\sigma}_{xy} = \sum_{\alpha=1}^{n} w^{\alpha} \mathbf{T}_{\sigma}^{-1}(\phi^{\alpha}) \mathbf{D}_{ns}^{\alpha} \mathbf{T}_{\varepsilon}(\phi^{\alpha}) \boldsymbol{\varepsilon}_{xy} \tag{34}$$

with n the chosen number of microplanes and w^{α} the weighting factors.

Attention is drawn to the fact that the second row of $\mathbf{D}_{ns}^{\alpha}$ consists of zeros. This is because in the microplane concept only the normal stress and the shear stress are resolved on each microplane. The normal stress parallel to this plane therefore becomes irrelevant. Furthermore, attention is drawn to the fact that here we use a relatively simple version of the microplane model, namely one in which no splitting in volumetric and deviatoric components is considered [15]. Nevertheless, more sophisticated microplane models, e.g. Ref. [16], which incorporates such a split, can be captured by the same formalism [26]. It is finally noted that the microplane is very similar to the multiple fixed-crack model [21,22], except for the fact that the multiple fixed-crack model has been formulated in terms of a strain decomposition.

For the fixed crack model, differentiation of Eq. (28) yields the tangential stress–strain relation needed in an incremental-iterative procedure which utilises the Newton–Raphson method:

$$\dot{\boldsymbol{\sigma}}_{xy} = \mathbf{T}_{\sigma}^{-1}(\phi_0)(\mathbf{D}_{ns}^{s} - \Delta\mathbf{D}_{ns}) \mathbf{T}_{\varepsilon}(\phi_0) \dot{\boldsymbol{\varepsilon}}_{xy} \tag{35}$$

with $\mathbf{D}_{ns}^{s}$ given by Eq. (26) and

$$\Delta\mathbf{D}_{ns} = \begin{bmatrix} d_{11} & 0 & 0 \\ v d_{11} & 0 & 0 \\ d_{31} & 0 & 0 \end{bmatrix} \tag{36}$$

with

$$d_{11} = \frac{\partial \omega_1}{\partial \kappa} \frac{\partial \kappa}{\partial \varepsilon_{nn}} \frac{E(\varepsilon_{nn} + v\varepsilon_{ss})}{(1 - (1 - \omega_1)v^2)^2}$$

and

$$d_{31} = \frac{\partial \omega_2}{\partial \kappa} \frac{\partial \kappa}{\partial \varepsilon_{nn}} G\gamma_{ns}$$

with $\partial\kappa/\partial\varepsilon_{nn} = 1$ upon loading and zero otherwise. We observe that the local material tangential stiffness matrix $\mathbf{D}_{ns}^{s} - \Delta\mathbf{D}_{ns}$ generally becomes non-symmetric.

In the rotating smeared crack model the local coordinate system of the crack and the principal axes of stress and strain coincide throughout the entire deformation process, which, as discussed, implies that the secant stiffness matrix $\mathbf{D}_{ns}^{s}$ relates principal stresses to principal strains, and that a secant shear stiffness becomes superfluous. Consequently, there is only one remaining damage parameter, $\omega_1 = \omega$, and we have

$$\mathbf{D}_{ns}^{s} = \begin{bmatrix} \frac{(1-\omega)E}{1-(1-\omega)v^2} & \frac{(1-\omega)vE}{1-(1-\omega)v^2} & 0 \\ \frac{(1-\omega)vE}{1-(1-\omega)v^2} & \frac{E}{1-(1-\omega)v^2} & 0 \\ 0 & 0 & 0 \end{bmatrix} \tag{37}$$

instead of expression (26). With Eq. (37) differentiation of the secant stiffness relation in global coordinates yields [17,27,28]:

$$\dot{\boldsymbol{\sigma}}_{xy} = \mathbf{T}_{\sigma}^{-1}(\phi)(\mathbf{D}_{ns}^{s} - \Delta\mathbf{D}_{ns}) \mathbf{T}_{\varepsilon}(\phi) \dot{\boldsymbol{\varepsilon}}_{xy} \tag{38}$$

with $\Delta\mathbf{D}_{ns}$ now given by

$$\Delta\mathbf{D}_{ns} = \begin{bmatrix} d_{11} & 0 & 0 \\ \nu d_{11} & 0 & 0 \\ 0 & 0 & d_{33} \end{bmatrix} \tag{39}$$

with

$$d_{11} = \frac{\partial\omega}{\partial\kappa}\frac{\partial\kappa}{\partial\varepsilon_{nn}}\frac{E(\varepsilon_{nn}+\nu\varepsilon_{ss})}{(1-(1-\omega)\nu^2)^2}$$

and

$$d_{33} = -\frac{\sigma_{nn}-\sigma_{ss}}{2(\varepsilon_{nn}-\varepsilon_{ss})}$$

The tangential stress–strain relation of the microplane model can be cast in the same formalism as that of the rotating and the fixed crack models. Indeed, upon linearisation of Eq. (34) we obtain

$$\dot{\boldsymbol{\sigma}}_{xy} = \sum_{\alpha=1}^{n} w^{\alpha}\mathbf{T}_{\sigma}^{-1}(\phi^{\alpha})(\mathbf{D}_{ns}^{\alpha} - \Delta\mathbf{D}_{ns}^{\alpha})\mathbf{T}_{\varepsilon}(\phi^{\alpha})\dot{\boldsymbol{\varepsilon}}_{xy} \tag{40}$$

with $\mathbf{D}_{ns}^{\alpha}$ given by Eq. (31) and $\Delta\mathbf{D}_{ns}^{\alpha}$ defined as

$$\Delta\mathbf{D}_{ns}^{\alpha} = \begin{bmatrix} d_{11}^{\alpha} & 0 & 0 \\ 0 & 0 & 0 \\ 0 & 0 & d_{33}^{\alpha} \end{bmatrix} \tag{41}$$

with

$$d_{11}^{\alpha} = \frac{\partial\omega_{\mathrm{N}}^{\alpha}}{\partial\kappa_{\mathrm{N}}^{\alpha}}\frac{\partial\kappa_{\mathrm{N}}^{\alpha}}{\partial\varepsilon_{nn}^{\alpha}}E_{\mathrm{N}}\varepsilon_{nn}^{\alpha}$$

where $\partial\kappa_{\mathrm{N}}^{\alpha}/\partial\varepsilon_{nn}^{\alpha} = 1$ if $f_{\mathrm{N}}^{\alpha} = 0$ and zero otherwise, and

$$d_{33}^{\alpha} = \frac{\partial\omega_{\mathrm{T}}^{\alpha}}{\partial\kappa_{\mathrm{T}}^{\alpha}}\frac{\partial\kappa_{\mathrm{T}}^{\alpha}}{\partial\gamma_{ns}^{\alpha}}E_{\mathrm{T}}\gamma_{ns}^{\alpha}$$

while $\partial\kappa_{\mathrm{T}}^{\alpha}/\partial\gamma_{ns}^{\alpha} = 1$ if $f_{\mathrm{T}}^{\alpha} = 0$ and zero otherwise.

4. Softening and energy concepts

4.1. Cohesive-zone models

A most important issue when considering failure of quasi-brittle materials is the observation that they are not perfectly brittle in the Griffith sense, but display some ductility after reaching the strength limit. In fact, there exists a small zone in front of the crack tip, in which initiation and coalescence of micro-cracks take place. If this so-called *fracture process zone* is sufficiently small compared to the structural dimensions, linear-elastic fracture mechanics concepts still apply. However, if this is no longer the case, the cohesive forces that exist in this fracture process zone must be taken into account, and so-called *cohesive-zone models* must be utilised. In such models, the degrading mechanisms in front of the crack tip are lumped into a discrete line, and a stress–displacement (σ–u) diagram over this line represents the softening effects in the fracture process zone (Fig. 2). Some examples of such stress-separation laws are given in Fig. 3 for a ductile material and a quasi-brittle material, respectively. Apart from the shape of the stress–displacement relation, also the area under it is material dependent. This area represents the fracture energy (G_{f}), i.e. the energy

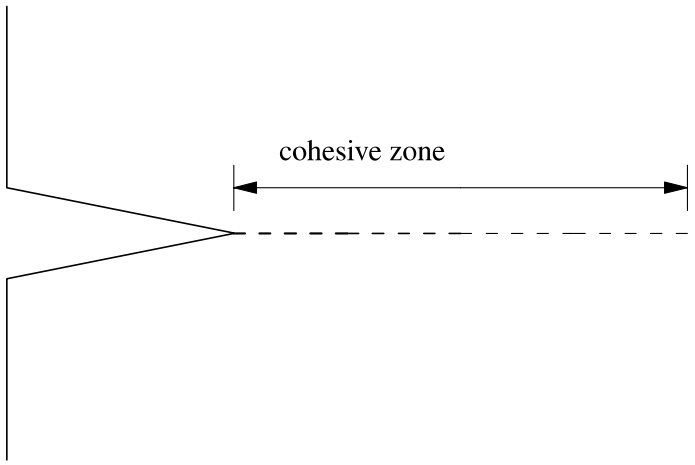

Fig. 2. Schematic representation of a crack tip and a cohesive zone.

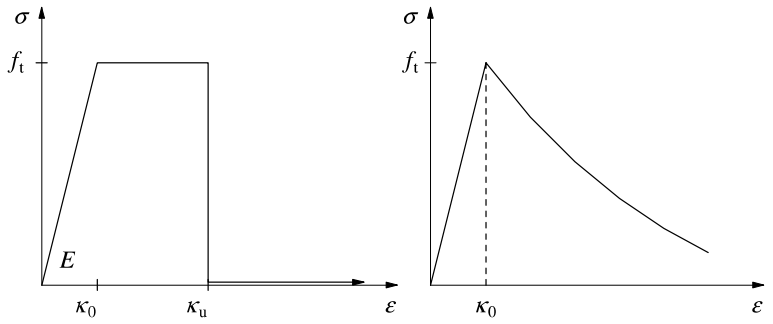

Fig. 3. Various possibilities for stress–displacement relations in a cohesive zone.

that is needed to create a unit area of fully developed crack. Formally, the definition of the fracture energy reads:

$$G_f = \int \sigma \, du \tag{42}$$

with σ and u the stress and the displacement across the fracture process zone. Cohesive-zone models were introduced around 1960 by Dugdale [8] and Barenblatt [9] for elastic–plastic fracture in ductile metals, and for quasi-brittle materials Hillerborg [10] published his so-called fictitious crack model for concrete, which ensured a discretisation-independent energy release upon crack propagation.

Adapting this concept to smeared formulations, Bažant and Oh [11] developed the crack band model, in which the fracture energy G_f was smeared out over the width of the area in which the crack *localises*, so that

$$G_f = \int \int \sigma \, d\varepsilon(x) \, dx \tag{43}$$

with x the ordinate orthogonal to the crack direction. When we assume that the strains are constant over a bandwidth w (an assumption commonly made in numerical analyses), we obtain

$$G_f = w g_f \tag{44}$$

with g_f the work dissipated per unit area of fully damaged material:

$$g_f = \int \sigma \, d\varepsilon \tag{45}$$

With the assumption of a uniform strain distribution and carrying out the integration of Eq. (45) for a linear softening diagram, we arrive at the following expression for the strain κ_u at which the residual strength is exhausted:

$$\kappa_u = \frac{2G_f}{f_t w} \tag{46}$$

We now consider the case of a one-dimensional bar of length L which is divided into m elements with a linear displacement interpolation. Since $w = L/m$, a softening modulus h can be derived as

$$h = -\frac{Lf_t^2}{2mG_f - Lf_t^2/E} \tag{47}$$

We observe that this modulus is proportional to the structural size and inversely proportional to the number of elements. In fact, a model in which the softening modulus was made a function of the element size has been proposed first by Pietruszczak and Mróz [29].

When we give one element a tensile strength that is marginally below that of the other elements, we can derive an expression for the average strain in the bar beyond the peak load:

$$\bar{\varepsilon} = \frac{\sigma}{E} + \frac{2G_f(f_t - \sigma)}{Lf_t^2} \tag{48}$$

We observe that the number of elements m has disappeared from this expression and inclusion of the fracture energy G_f has thus made the stress–average strain curve, or equivalently, the load–displacement curve, insensitive with regard to mesh refinement. Simultaneously, the specimen length L has entered the expression for the average strain $\bar{\varepsilon}$, so that the brittleness of the structure depends on the value of L, and a size effect is present in the formulation.

In two and three-dimensional finite element calculations the global load–displacement response does not become completely insensitive with respect to the discretisation as in the above one-dimensional example. This is partly due to the fact that it is difficult to estimate the value of the band width w. Especially if the crack propagates at an angle with the mesh lines, a proper estimate for w can be difficult. Often, it is assumed that the width over which the fracture energy is distributed can be related to the area of an element A_{elem} [17,18,30]:

$$w = \alpha\sqrt{A_{elem}} = \alpha\sqrt{\sum_{i=1}^{NINT} \gamma_i \det \mathbf{J}_i} \tag{49}$$

with γ_i the weight factors of the integration rule and $\det \mathbf{J}_i$ the Jacobian of the transformation between the local, isoparametric coordinates and the global coordinate system in integration i. The factor α is a modification factor which depends on the element type and the integration scheme.

Recently, finite element models with embedded discontinuities have become popular. There are two versions of these models, namely the strong discontinuity approach [31–33] and the weak discontinuity approach [34–36]. We will depart from the latter approach and define an element, see Fig. 4, in which a band is defined within the element where the strains are different in magnitude than the strains in the remainder of the element:

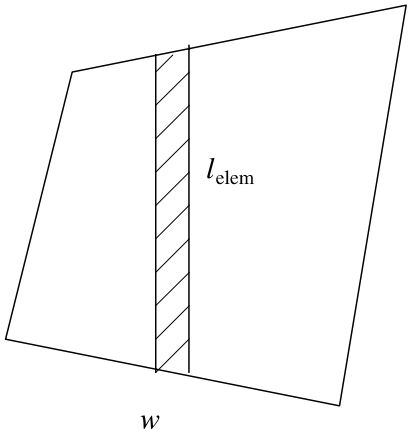

Fig. 4. Embedded discontinuity in a finite element.

$$\varepsilon_{ij}^{+} = \bar{\varepsilon}_{ij} + \frac{\alpha^{+}}{2}(n_i m_j + n_j m_i) \tag{50}$$

and

$$\varepsilon_{ij}^{-} = \bar{\varepsilon}_{ij} + \frac{\alpha^{-}}{2}(n_i m_j + n_j m_i) \tag{51}$$

with $\mathbf{n}$ a vector normal to the band and $\mathbf{m}$ related to the deformation mode, e.g., $\mathbf{m} = \mathbf{n}$ for mode-I behaviour and $\mathbf{n}$ orthogonal to $\mathbf{m}$ for mode-II behaviour. α^{+} and α^{-} are scalars indicating the magnitude of the strain inside and outside of the band, respectively, measured relative to the average, continuous strain $\bar{\boldsymbol{\varepsilon}}$ in the element. The stress–strain relation in the band can now be specified independently from that in the bulk of the element. Typically, a softening relation is prescribed which results in an energy dissipation per unit volume g_{f} (Eq. (45)) upon complete loss of material coherence. For a band with a width w, which is incorporated in the finite element formulation, we thus retrieve the fracture energy that

$$G_{\text{f}} = w \int \sigma \, \mathrm{d}\varepsilon \tag{52}$$

that is dissipated for the creation of a unit area of fully developed crack.

A problem resides in the determination of the length of the crack band, l_{elem} in a specific element. Obviously, for a given length l_{elem} the total energy dissipation in an element reads

$$G_{\text{f,elem}} = l_{\text{elem}} G_{\text{f}} \tag{53}$$

If the crack length in an element is estimated incorrectly, the energy that is dissipated in each element is also wrong, and so will be the total load-displacement diagram [36]. Different possibilities exist, e.g. to relate l_{elem} to the area of the element A_{elem} in the spirit of Eq. (49) [35]. Other possibilities are to assume that the enhanced mode passes through the element midpoint [31], and to calculate the band length accordingly, or to let the band connect at the element boundaries and to compute the band length in this fashion [33].

While the above considerations have been set up for the so-called weak discontinuity approach, in which the displacement is continuous, it is also possible to let the enhanced strain modes (second part of the right-hand side of Eqs. (50) and (51)) be unbounded. This so-called strong discontinuity approach can be conceived as a limiting case of the weak discontinuity approach for $w \to 0$. The strain then locally attains the form of a Dirac function and the displacement becomes discontinuous over a single discrete plane.

Consistent with the properties of a Dirac function, the integral over time of the product of the stress and the difference in strain rates at both sides still equals the fracture energy [37].

Although the embedded discontinuity approaches, either in the weak form or in the strong form, definitely enhance the deformational capabilities of the elements, so that the strong local strain gradients inside crack bands are better captured, it is emphasised that the fundamental problem of loss of well-posedness of the boundary-value problem is not solved in this manner [38].

4.2. Compressive softening

In the literature, the uniaxial compressive stress–strain behaviour can be approximated by different functions, e.g. [39,40]. However, these relations are usually not energy-based formulations, and thus suffer from the same excessive dependency on the fineness of the discretisation as when tension-softening models are utilised which do not incorporate a fracture energy. Feenstra [17,19] has suggested to model the behaviour in compression with a compression softening model in which, similar to the crack band model for tensile loadings, a compressive fracture energy is introduced, G_c. For instance, the equivalent stress–equivalent strain diagram then reads [17,19]

$$\bar{\sigma}_c(\kappa_c) = \begin{cases} \frac{f_c}{3}\left(1 + 4\frac{\kappa_c}{\kappa_{ec}} - 2\frac{\kappa_c^2}{\kappa_{ec}^2}\right) & \text{if } \kappa_c < \kappa_{ec} \\ f_c\left(1 - \frac{(\kappa_c - \kappa_{ec})^2}{(\kappa_{uc} - \kappa_{ec})^2}\right) & \text{if } \kappa_{ec} \leqslant \kappa_c < \kappa_{uc} \end{cases} \tag{54}$$

with κ_c an internal damage parameter and f_c the compressive strength, see also Fig. 5. The maximum compressive strength will be reached at an equivalent strain κ_{ec} which is independent of the element size w and reads

$$\kappa_{ec} = \frac{4}{3}\frac{f_c}{E_c} \tag{55}$$

with E_c the Young's modulus of the concrete. The quintessence of this compression-equivalent of the crack band model is that the maximum equivalent strain κ_{uc} is related to the compressive fracture energy G_c and the element size as follows,

$$\kappa_{uc} = \frac{3G_c}{2wf_c} \tag{56}$$

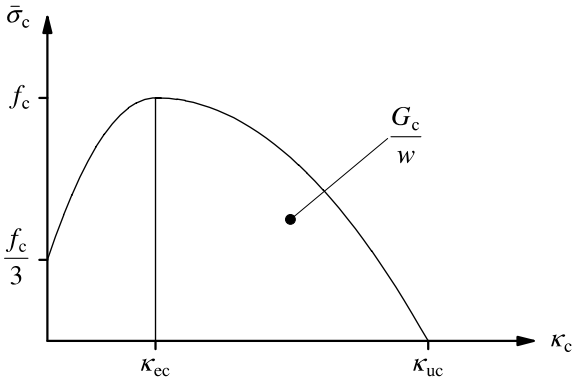

Fig. 5. Energy-based equivalent stress–strain diagram for compression.

Experimental evidence for the assumption that the compressive fracture energy G_c can be considered as a material parameter has been provided by Vonk [41].

5. On reinforced concrete modelling

The tension-stiffening effect is usually understood as the ability to gradually redistribute the load in a structure from concrete to steel under the formation of primary and secondary cracks. As discussed before, tension-stiffening models which lump the stiffness increase of the intact concrete between the cracks to the concrete properties, result in a softening branch. This is potentially confusing, since the tension-softening models also result in a descending branch in the concrete stress–strain diagram. Obviously, the physical basis of the latter class of models is totally different. In a transparent approach, Feenstra [17,42] has suggested to conceive the tension-stiffening effect as the additional stiffness due to the interaction between concrete and reinforcement in the direction of the reinforcement, and to model the formation of primary and secondary cracks with the constitutive model of plain concrete in tension, for instance the crack band model. In the presence of reinforcement the fracture-energy in this model is distributed over a tributary area by using the crack spacing as formulated in the CEB–FIP model code [40].

In reinforced concrete a number of cracks usually develop during the process of loading until the cracking process stabilises and no further cracks develop in the structure. The crack spacing at stabilised cracking is determined mainly by the amount of reinforcement. A rational assumption is that the material model for plain concrete, e.g., based on fracture energy G_f of a single crack, can be applied to reinforced concrete with the total amount of fracture energy dissipated over the average crack spacing l_s. Because the fracture energy is assumed to be a material parameter, only the average crack spacing l_s has to be determined. Normally, the dimensions of the finite elements, w, in simulations of reinforced concrete structures are much larger than the average crack spacing l_s. Bearing this in mind, it is reasonable to assume that the released energy in reinforced concrete, G_f^{rc}, can be determined by

$$G_f^{rc} = \min\left\{G_f, G_f \frac{w}{l_s}\right\} \tag{57}$$

The average crack spacing is a function of the bar diameter, the concrete cover and the reinforcement ratio, and can be estimated according to the CEB–FIP model code [17,40,42].

Following Feenstra [17,42] it is assumed that the behaviour of cracked, reinforced concrete can be obtained by superposition of the stiffness of plain concrete, a stiffness of the reinforcement and an additional stiffness due to interaction between concrete and reinforcement. This leads to the following summation of stress contributions

$$\boldsymbol{\sigma} = \boldsymbol{\sigma}_c + \boldsymbol{\sigma}_s + \boldsymbol{\sigma}_{ia} \tag{58}$$

with $\boldsymbol{\sigma}_c$ the stress contribution of the plain concrete, $\boldsymbol{\sigma}_s$ the contribution of the reinforcement, and $\boldsymbol{\sigma}_{ia}$ the interaction stress contribution due to tension-stiffening, Fig. 6 (left).

The constitutive model of the reinforcement is normally assumed to be given by an elasto-plastic model with a stiffness matrix given by

$$\mathbf{D}_s = \begin{bmatrix} \rho_p E_s^{ep} & 0 & 0 \\ 0 & \rho_q E_s^{ep} & 0 \\ 0 & 0 & 0 \end{bmatrix} \tag{59}$$

in which ρ_p and ρ_q are the reinforcement ratios in the p and q-directions, respectively. E_s^{ep} is the elasto-plastic modulus of the reinforcement. The shear stiffness of the reinforcing grid is assumed to be equal to zero. The stress contribution in the global x, y-coordinate system is computed via

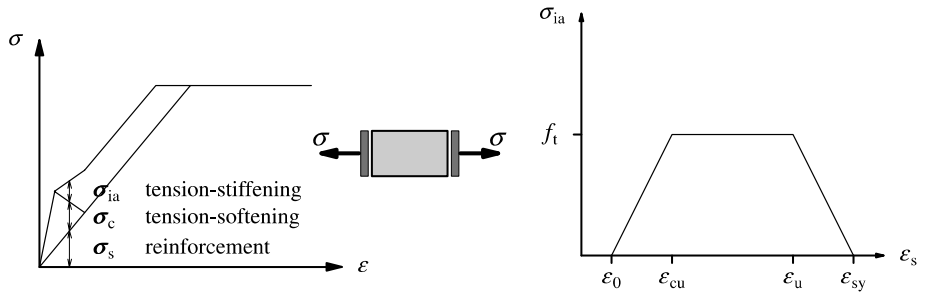

Fig. 6. Idealised representation of the constitutive model for concrete (left) and adopted tension-stiffening diagram for the interaction stress (right).

$$\boldsymbol{\sigma}_{\mathrm{s}} = [\mathbf{T}^{\mathrm{T}}(\psi)\mathbf{D}_{\mathrm{s}}\mathbf{T}(\psi)]\boldsymbol{\varepsilon} \tag{60}$$

with $\boldsymbol{\varepsilon}$ the strain vector in the global x, y-coordinate system and $\mathbf{T}(\psi)$ the standard transformation matrix between two coordinate systems, ψ being the angle between the x-axis and the main reinforcement p-axis.

After a stabilised crack pattern has developed, stresses are still transferred from reinforcement to concrete between the cracks due to the bond action which increases the total stiffness of the structure, Fig. 6 (left). The additional stress due to tension-stiffening is assumed to be given as a function of the strain in the direction of the reinforcement [43]. The interaction stress is assumed to be given by a trilinear function according to Cervenka et al. [44], Fig. 6 (right). The interaction stress is only active if the strain in the reinforcement is larger than ε_0 which is determined by

$$\varepsilon_0 = \frac{f_{\mathrm{t}}}{E_{\mathrm{c}}}\cos^2\delta \tag{61}$$

with δ the angle between the direction of the reinforcement and the direction of the principal stress at incipient cracking. The strain $\varepsilon_{\mathrm{cu}}$ is determined by the crack spacing, the equivalent length of the element and the fracture energy of the concrete and is given by

$$\varepsilon_{\mathrm{cu}} = 2\cos^2\delta\frac{G_{\mathrm{f}}^{\mathrm{rc}}}{wf_{\mathrm{t}}} \tag{62}$$

The constant part of the diagram can be approximated by the tensile strength of the concrete. The tension-stiffening component is reduced near the yield strain of the reinforcement $\varepsilon_{\mathrm{sy}}$ in order to avoid an artificial increase of the yield stress of the reinforcement. The strain at which the tension-stiffening component is reduced is given by

$$\varepsilon_{\mathrm{u}} = \varepsilon_{\mathrm{sy}} - \frac{f_{\mathrm{t}}}{\rho_{\mathrm{s,eff}}E_{\mathrm{s}}} \tag{63}$$

with $\rho_{\mathrm{s,eff}}$ the effective reinforcement ratio [17,40,42].

The local stiffness matrix that incorporates the interaction stiffness is then given by

$$\mathbf{D}_{\mathrm{ia}} = \begin{bmatrix} E_{\mathrm{b},p} & 0 & 0 \\ 0 & E_{\mathrm{b},q} & 0 \\ 0 & 0 & 0 \end{bmatrix} \tag{64}$$

in which $E_{\mathrm{b},p}$ and $E_{\mathrm{b},q}$ the bond stiffnesses in the p and q-directions of the grid, respectively. The transformation to the global coordinate system again follows from

$$\boldsymbol{\sigma}_{\mathrm{ia}} = [\mathbf{T}^{\mathrm{T}}(\psi)\mathbf{D}_{\mathrm{ia}}\mathbf{T}(\psi)]\boldsymbol{\varepsilon} \tag{65}$$

6. Concluding remarks

In this contribution an overview has been given of some of the more important developments in smeared finite element analyses of fracture in quasi-brittle materials, with an emphasis on plain and reinforced concrete. No completeness is claimed, and important issues like time-dependence have been left out.

References

[1] Rashid YR. Analysis of prestressed concrete pressure vessels. Nucl Engng Des 1968;7:334–44.
[2] Ngo D, Scordelis AC. Finite element analysis of reinforced concrete beams. J Am Concr Inst 1967;64:152–63.
[3] Suidan M, Schnobrich WC. Finite element analysis of reinforced concrete. ASCE J Struct Div 1973;99:2109–22.
[4] Cope RJ, Rao PV, Clark LA, Norris P. Modelling of reinforced concrete behaviour for finite element analysis of bridge slabs. In: Taylor C, Hinton E, Owen DRJ, editors. Numerical methods for non-linear problems. Swansea: Pineridge Press; 1980. p. 457–70.
[5] Cedolin L, Bažant ZP. Effect of finite element choice in blunt crack band analysis. Comp Meth Appl Mech Engng 1980;24:305–16.
[6] Bažant ZP. Instability, ductility and size effect in strain softening concrete. ASCE J Engng Mech 1976;102:144–331.
[7] Crisfield MA. Local instabilities in the non-linear analysis of reinforced concrete beams and slabs. Proc Instn Civ Engrs Part 2 1982;73:135–45.
[8] Dugdale DS. Yielding of steel sheets containing slits. J Mech Phys Solids 1960;8:100–8.
[9] Barenblatt GI. The mathematical theory of equilibrium cracks in brittle fracture. Adv Appl Mech 1962;7:55–129.
[10] Hillerborg A, Modeer M, Petersson PE. Analysis of crack formation and crack growth in concrete by means of fracture mechanics and finite elements. Cement Concr Res 1976;6:773–82.
[11] Bažant ZP, Oh B. Crack band theory for fracture of concrete. RILEM Mat Struct 1983;16:155–77.
[12] Mazars J. Application de la mécanique de l'endommagement au comportement non linéare et à la rupture du béton de structure. These d'Etat. Paris: Université Paris VI, 1984.
[13] Mazars J, Pijaudier-Cabot G. Continuum damage theory—application to concrete. ASCE J Engng Mech 1989;115:345–65.
[14] Batdorf SB, Budiansky B. A mathematical theory of plasticity based on the concept of slip. NACA Tech Note 1871, 1949.
[15] Bažant ZP, Gambarova P. Crack shear in concrete: crack band microplane model. ASCE J Struct Engng 1984;110:2015–36.
[16] Bažant ZP, Prat PC. Microplane model for brittle plastic material. I. Theory and II. Verification. ASCE J Engng Mech 1988;114:1672–702.
[17] Feenstra PH. Computational aspects of biaxial stress in plain and reinforced concrete. Dissertation, Delft: Delft University of Technology; 1993.
[18] Feenstra PH, de Borst R. A plasticity model for mode-I cracking in concrete. Int J Num Meth Engng 1995;28:2509–29.
[19] Feenstra PH, de Borst R. A composite plasticity model for concrete. Int J Solids Struct 1996;33:707–30.
[20] Kolmar W, Mehlhorn G. Comparison of shear stiffness formulations for cracked reinforced concrete elements. In: Damjanić F, et al., editors. Proceedings of International Conference on Computer Aided Analysis and Design of Concrete Structures, Part 1, Swansea: Pineridge Press; 1984. p. 133–47.
[21] de Borst R, Nauta P. Non-orthogonal cracks in a smeared finite element model. Engng Comput 1985;2:35–46.
[22] de Borst R. Smeared cracking, plasticity, creep and thermal loading—a unified approach. Comp Meth Appl Mech Engng 1987;62:89–110.
[23] Rots JG. Computational modeling of concrete fracture. Dissertation. Delft: Delft University of Technology; 1988.
[24] Lemaitre J, Chaboche JL. Mechanics of solid materials. Cambridge: Cambridge University Press; 1990.
[25] de Vree JHP, Brekelmans WAM, van Gils MAJ. Comparison of non-local approaches in continuum damage mechanics. Comp Struct 1995;55:581–8.
[26] Kuhl E, Ramm E. On the linearization of the microplane model. Mech Coh-frict Mat 1998;3:343–64.
[27] Bažant ZP. Comment on orthotropic models for concrete and geomaterials. ASCE J Engng Mech 1983;109:849–65.
[28] Willam K, Pramono E, Sture S. Fundamental issues of smeared crack models. In: Shah SP, Swartz SE, editors. Proc Conf Fracture Concrete and Rock, SEM/RILEM, 1986. p. 142–57.
[29] Pietruszczak S, Mróz Z. Finite element analysis of deformation of strain softening materials. Int J Num Meth Engng 1981;17: 327–34.
[30] Willam K. Experimental and computational aspects of concrete fracture. In: Damjanić F, et al., editors. Proceedings of International Conference on Computer Aided Analysis and Design of Concrete Structures, Part 1, Swansea: Pineridge Press; 1984. p. 33–70.
[31] Simo JC, Oliver J, Armero F. An analysis of strong discontinuities induced by softening relations in rate-independent solids. Comp Mech 1993;12:277–96.

[32] Larsson R, Runesson K, Ottosen NS. Discontinuous displacement approximation for capturing plastic localization. Int J Num Meth Engng 1993;36:2087–105.
[33] Lotfi HR, Shing PB. Embedded representation of fracture in concrete with mixed elements. Int J Num Meth Engng 1995;38: 1307–25.
[34] Ortiz M, Leroy Y, Needleman A. A finite element method for localized failure analysis. Comp Meth Appl Mech Engng 1987;61:189–214.
[35] Belytschko T, Fish J, Engelman BE. A finite element with embedded localization zones. Comp Meth Appl Mech Engng 1988;70:59–89.
[36] Sluys LJ, Berends AH. Discontinuous failure analysis for mode-I and mode-II localization problems. Int J Solids Struct 1998;35:4257–74.
[37] Oliver J, Cervera M, Manzoli O. On the use of strain-softening models for the simulation of strong discontinuities in solids. In: de Borst R, van der Giessen E, editors. Material instabilities in solids. Chichester: Wiley; 1998. p. 107–23.
[38] de Borst R, Sluys LJ, Mühlhaus H-B, Pamin J. Fundamental issues in finite element analysis of localisation of deformation. Engng Comput 1993;10:99–122.
[39] Vecchio FJ, Collins MP. The response of reinforced concrete to in-plane shear and normal stresses. Publication 82-03, Toronto: University of Toronto; 1982.
[40] CEB-FIP. Model Code 1990. Bulletin d'Information, Lausanne, 1990.
[41] Vonk R. Softening of concrete loaded in compression. Dissertation. Eindhoven: Eindhoven University of Technology; 1992.
[42] Feenstra PH, de Borst R. A constitutive model for reinforced concrete. ASCE J Engng Mech 1995;121:587–95.
[43] Floegl H, Mang HA. On tension stiffening in crack reinforced concrete slabs and shells considering geometric and physical nonlinearity. Ing Arch 1981;51:215–30.
[44] Cervenka V, Pukl R, Eligehausen R. Computer simulation of anchoring technique in rein-forced concrete beams. In: Bićanić N, Mang HA, editors. Computer Aided Analysis and Design of Concrete Structures. Swansea: Pineridge Press; 1990. p. 1–21.
[45] Peerling RHJ, de Borst R, Brekelmans WAM, Geers MGD. Gradient-enhanced damage modelling of concrete fracture. Mech Coh-frict Mat 1998;3:323–42.